Effect of fractures on hot solvent injection in viscous oil: a study using HP-HT micromodel

Igor Bondino[1,*], *Gerardo Emanuel* Romero[1], *Jean-Philippe* Chaulet[1], *Anne* Brisset[1] and *Marelys* Mujica[2]

[1]TOTAL, Avenue Larribau, 64018 Pau Cedex, France
[2]CHLOE, Avenue de l'Université, UFR Sciences et Techniques, 64013 Pau Cedex, France

Abstract. In this study, a transparent glass micromodel is used to study the physico-chemical behaviour of a solvent / viscous oil system with pressures and temperatures in the range [8-100] bar and [60-110] °C respectively, allowing the visual observation of the phenomena at the actual P, T reservoir conditions of interest. The experiments, covering immiscible, miscible and supercritical conditions, reveal the influence of pressure, temperature, connate water and fractures, on the oil recovery and flow behaviour. A physico-chemical interpretation is performed, by both analytical and numerical methods, resulting in deep understanding of the miscible process at microscopic scale. It is found that the most interesting behaviour in terms of oil recovery (for the type of solvent used in this work) is given by the ratio of fracture permeability to intact matrix permeability (which is commonly referred to as excess permeability index). Being the micromodel vertically oriented with the lighter solvent injected from the top, the stability of the experiments is also classified: although solvent fingers are expected as buoyancy is not strong enough to prevent their initiation and growth, in reality they are only seen in a minority of experiments. This behaviour is explained due to the contributions of the transverse dispersion (which smooths out the fingers as they grow) and to the fractures on the stabilization of the flow inside the matrix.

1 Introduction

Miscible-flood studies started in the early 1950's. Since then, several improvements have been achieved to make miscible flooding economical and technically applicable. By consequence, more complex processes such as miscible WAG, CO2 miscible displacement and foam addition have been applied at reservoir scale. Solvent injection can be used as a secondary or tertiary oil recovery method and is normally implemented in order to achieve miscible displacement, which implies that the solvent and reservoir fluid mix in all proportions and that all mixtures remain in single phase. This also means absence of interfacial tension, hence no capillary pressure and no interface. However, miscible injection has not been as widely applied as water flooding due to process and solvent cost or solvent availability issues: for example, the incremental oil recovery must be sufficiently large and timely to withstand the added operational costs. Obviously such evaluation requires a good understanding of the mechanisms: but the processes that happen in a reservoir at microscopic scale and in-situ conditions of pressure and temperature, are still not very well understood.

The micromodel technology remains today the best tool to visualize the physico-chemical behaviour of a solvent/oil system at different conditions. A large set of investigations was for example carried out for the specific problem of heavy oil recovery by means of vaporized hydrocarbon solvents, VAPEX (see Chatzis [1] for one of the early examples). A micromodel is an idealized transparent representation of a rock to visualize how a recovery mechanism works at a pore scale. The principle of a micromodel experiment is similar to that of a traditional core flooding experiment, with the exception that the pore pattern is manmade and 2D and that the volumes involved are very small (tens to a few hundred microliters). State-of-the-art optical cameras (as in this paper) can be used to capture the fluid displacements within the pore network while the displacing fluid is injected. A number of investigators have used this tool for solvent studies.

Campbell and Orr [2] studied the injection of CO2 and refined oil respectively, at 8.3 bar and 25°C in crude and refined oil. The experiments were conducted in water-wet and oil-wet media. It was found that oil gets trapped in the region that was first penetrated by the viscous fingers. This is due to oil's impoverishment and loss of its miscible condition. For refined oil as solvent, the oil-wet medium facilitates the residual oil/solvent contact as the crude oil wets the pore walls while the solvent passes through them. In the water-wet medium, CO2 dissolves in water and reaches out more trapped oil, reducing its viscosity and allowing it to be produced. Crude oil/CO2 systems are not first contact miscibility, and present capillary forces that favour the removal of oil from dead end pores, which increases the recovered oil.

* Corresponding author: igor.bondino@total.com

Sohrabi et al. [3] observed the performance of gravity stable CO2 injection for extra-heavy crude oil at 41.46 bar and 44°C, applying different sequences of water-alternating-gas injection (WAG). Starting with CO2 injection, the highest recovery factor is obtained after the first CO2/water cycle, where oil swelling is observed. CO2 displaces oil by a double drainage mechanism, which means gravity stable displacement of the solvent while dissolving into the oil and reducing its viscosity. Gravity stability refers to the inhibition of fingers formation due to a compensation of the viscous forces with gravity forces.

Saidian et al. [4] investigate the matrix-fracture interaction in glass micromodels during miscible displacement considering different injection rates, viscosity ratios and solvents. It is demonstrated that oil recovery increases with injection rate when the oil/solvent viscosity ratio equals one. But when the viscosity ratio is greater than one, the ultimate oil recovery decreases when the injection rate increases. This is due to the channelization of the solvent in the fracture that leaves the fracture-matrix interaction as diffusion dominated. One conclusion is that the viscosity ratio affects the "dispersion" in the matrix and in the fractures: nevertheless, considering the mixing-cell theory [5], dispersion refers to a phenomenon that happens in a porous medium and the term does not apply for the observations in the fracture. However, for the matrix only, dispersion increases when the viscosity ratio (oil/solvent) decreases.

Marciales and Babadagli [6] analyse the solvent retrieval process at atmospheric conditions for different wettabilities using two types of solvent: heptane and distilled oil. In their case, the micromodel has fractures and the process is non isothermal. It is observed that solvent entrapment is more frequent in non-oil wet media than in oil-wet media (no water saturation is present). This behaviour is explained considering the stability of the solvent film that forms on the pore walls of the oil-wet media. This allows the interconnection of the solvent drops and their flow. In oil-wet media, the solvent gets into the smaller pores and oil recovery increases. Distilled oil is proved to be more efficient for heavy oils.

Shokrlu and Babadagli [7] studied the formation of residual oil (kerosene) saturation for solvent injection (n-heptane) after and before water injection (WAG) at ambient conditions. It was concluded that solvent injection before any water injection increases drastically the oil recovery. Moreover, in order to prevent viscous instabilities, it was proposed that water injection should be always performed after solvent injection. Otherwise, viscous fingers form and recovered oil may decrease.

Qi et al. [8] analysed the condensing solvent extraction process, using propane and butane for bitumen extraction at pressures from 3 bar to 18 bar and temperatures from 70°C to 115°C, applying different flow rates. Three regions were identified: (1) vapor-solvent chamber, (2) condensing edge, (3) liquid solvent zone: the highest recovery factor was observed in zone (2) by a combination of bitumen dilution and vapour fingering.

Furthermore, interesting observations also emerge from literature on core experiments, as follows. Burger and Mohanty [9] analysed the mass transfer mechanisms from bypassed zones during gas injection, for a homogeneous and a heterogeneous core with different orientations and different enrichment levels of C3H8. The conditions were: miscible, first contact miscibility (FCM) and multi-contact miscibility (MCM), near-miscible and immiscible. It was then proved that the higher the enrichment level, the higher the recovery factor. Orientation affects the performance of the tests, which are dominated by different mass transfer mechanisms: gravity driven, capillary driven and so on. For horizontal orientation, MCM tests give higher recovery factors than FCM due to less gravity override.

Wylie and Mohanty [10] describe the gas injection as two in-series processes: gas flooding and oil bypassing, and mass transfer from the bypassed oil. Therefore, the impact of wettability on each is studied. Mass transfer is enhanced under oil-wet conditions (OW) and it is less effective as capillary forces increase. In OW, water saturation does not greatly affect mass transfer because it occupies the larger pores and does not block the flowing gas from contacting the oil. For OW, vertical gas flood (VGF), gravity stable, has a slightly lower recovery than for water-wet (WW). Horizontal gas flood (HGF) has lower recovery than VGF due to gravity override. For HGF, recovery increases monotonically with solvent enrichment for OW, while it barely increases for WW. This is the most remarkable conclusion and it is explained hypothesizing that water is redistributed in WW and shields the oil-solvent contact, while it remains trapped in the larger pores in OW.

Hopstaken [11] tested CO2, N2 and flue gas injection for a natural fractured reservoir core at (a) miscible and (b) immiscible conditions and different orientations. The lower recovery factor was obtained at immiscible conditions. When vertically oriented, the increase of the core size was proved to influence gravity forces and improve the recovery. Gravity drainage and mixing are the proposed mechanisms responsible for enhancing the recovery, while the oil entrapment due to capillary hold is pointed to diminish it.

From this literature analysis on microscopic recovery we therefore notice that solvent injection at microscopic scale presents still some questions, mainly on how the reservoir parameters, like water presence, wettability, pore pattern, fractures presence and type of solvent, impact on the behaviour of the fluid flow and the recovery at microscopic scale.

The objective of this paper is to provide a qualitative interpretation, from a physical and chemical point of view, of the results from 8 high pressure high temperature (HP-HT) micromodel experiments to determine the effects of temperature, pressure, connate water saturation, and fractures at reservoir conditions: HP-HT conditions were simultaneously applied on micromodels whose pore patterns have complex pore geometry and fractures. Each parameter was tested separately to give a thorough description of microscale solvent performance at reservoir conditions for continuous solvent injection.

2 Materials and methods

2.1. Micromodels

Three types of micromodels were manufactured by S.A.S KLEARIA (France) and utilized here (see also tables 1 and 2):

1. "Sandstone-like" with 28 inlets/outlets and 3 fractures spaced by 2.5cm (Chip 1).
2. "Sandstone-like" with 20 inlets/outlets and 3 fractures spaced by 2.5cm (Chip 2).
3. "Bi-modal carbonate-like" with 20 inlets/outlets and 2 larger than above fractures spaced by 5 cm (Chip 3)

The typical channel's cross section of glass (wet-) etched micromodels is shown in figure 1: fractures also have this characteristic cross section.

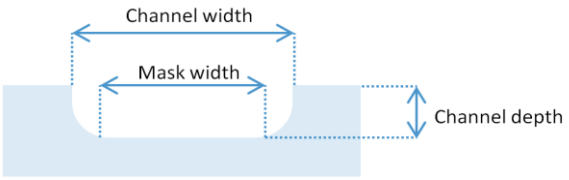

Fig. 1. Typical pore cross section in a glass micromodel (by wet etching technique): the pore cross section is not a true rectangle but a half ellipsoid due to acid etching.

Table 1. Characteristics of pore matrix dimensions.

	Chip 1, 2	Chip 3	
		Matrix-1 (macro pores)	Matrix-2 (micro pores)
Channel depth	40 µm	40 µm	1 µm
Mask width	40-320 µm	75-200 µm	10 µm Constant value everywhere

2.1.1. Sandstone-like micromodels (Chips 1 and 2)

Chips 1 and 2 are essentially equal, the sole difference lies in the amount and size of inlets/outlets. Chip 2 has fewer inlets/outlets but they are wider. This change was made during the course of the experimental program and allowed the viscous fluid to flow more easily during the oil saturation phase facilitating the set-up of the test.

The matrix pattern (figure 2) was created by repeating periodically an identical "tile" of dimensions approximately 3mmx3mm, derived from a 2D slice of a x-ray tomography dataset of 1 Darcy Clashach sandstone, which was manually edited, on a subjective empirical basis, to enhance its connectivity and guarantee percolation in the 2D space.

The pore pattern, excluding inlet/outlet channels, has size 5 cm x 5 cm x 40 µm (length x width x depth), and is constituted by D263 glass. The pore volume was experimentally estimated to be around 150 µl, without inlet/outlet channels. Permeability was not measured experimentally: but matrix permeability was estimated using CFD simulation, as will be explained in Section 5.

Table 2. Position of fractures and their dimensions. The three blue lines indicate the positions of the fractures in Chips 1 and 2 whilst the thicker red lines give the position in Chip 3.

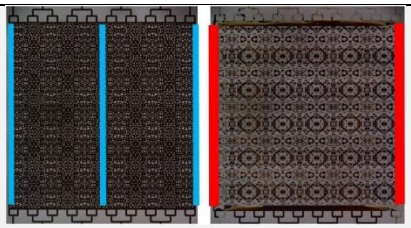

	Chips 1 and 2	Chip 3
Channel depth	40 µm	40 µm
Mask width	200 µm	1000 µm
Channel width	280 µm	1080 µm

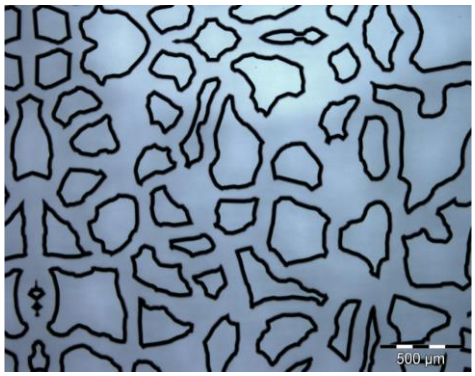

Fig. 2. Optical microscope image of pore pattern (Chips 1 & 2).

2.1.2. Bi-modal carbonate-like micromodels

The matrix pattern was created from a 2D slice of a x-ray tomography dataset of a 250mD Estaillades limestone, similarly to what explained above: in this case though the x-ray dataset produced only a representation of the intergranular porosity (and not of the intragranular microporous regions). As before, the image was treated digitally in order to qualitatively reproduce two types of porosities, which we name for convenience as "macro-porosity" and "micro-porosity" (figure 3). The macro-pores alone (which are represented by the thick black lines in figure 3) do not form a connected percolating pore network. It is the "micro-porosity" that assures global percolation (see figure 4 for details of mask construction). The pore pattern dimensions are identical to Chips 1 and 2 (5cmx5cm). Pore volume and permeability were not estimated.

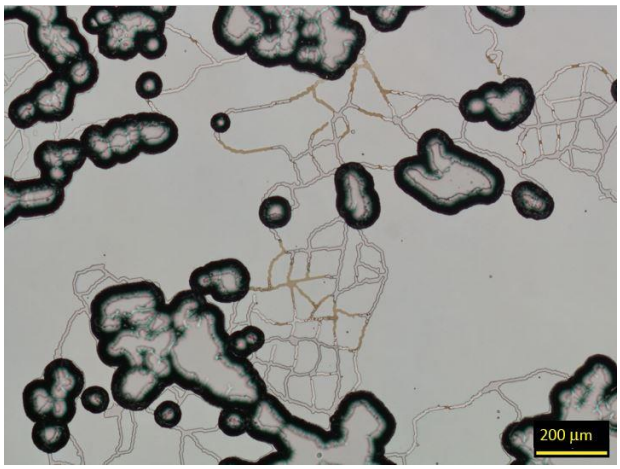

Fig. 3. Optical microscope image of pore pattern (Chip 3). Picture taken at the end of the experiment in a region close to a fracture: some residual oil is visible in the "micro-porosity" channels.

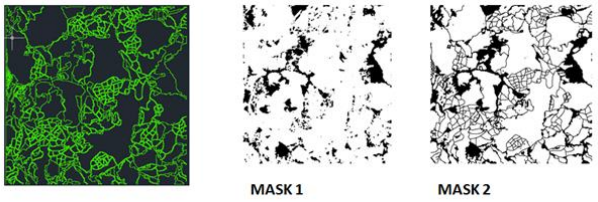

Fig. 4. Chip 3: on the left, the construction mask ("tile") of dimensions ~4mmx4mm that was repeated periodically across the 5cmx5cm surface of the pore pattern. The green lines track the contours of the porous system. The final "tile" (and micromodel) is actually composed by joining together the etched sides of two glass plates, one etched with pore depth 40um (from Mask 1) and one with depth 1um (from Mask 2).

2.1.3. Fractures

Chips 1 and 2 have three fractures (see table 2), parallel to the flow, which can be considered as channel type open aperture fracture [12]: two smooth fractures at each side of the pore pattern and a non-smooth one in the center (bounded by the rounded pore shapes of the matrix). The fractures' size is 0.2 mm, categorized as "capillary fractures" [13]. The fracture to matrix permeability ratio is estimated to be around 3 (matrix permeability was assessed using CFD software as explained in section 5). Chip 3 has only two smooth fractures at the sides, but of larger diameter (1mm, "supercapillary fracture"): the fracture to matrix permeability ratio is not available as the same image analysis and numerical CFD approach could not be used for this more complex matrix. In terms of behavior characterization of the systems under exam, considering the three fractures of Chip 1 and 2 and corresponding matrix, we can write the following flow equation:

$$Q = \Delta P \left(\frac{3}{8} \frac{\pi r^4}{\mu L} + \frac{k A}{\mu \Delta x} \right) \quad (1)$$

Which can be written as:

$$Q = \Delta P \left(\frac{1}{{8 \mu L}/{3 \pi r^4}} + \frac{1}{{\mu \Delta x}/{k A}} \right) = \frac{\Delta P}{{8 \mu L}/{(3 \pi r^4 + 8 k A)}} \quad (2)$$

For Chip 3, the bimodal pore matrix has two types of permeability acting in series and two parallel fractures along with the flow direction. The corresponding flow equation becomes:

$$Q = \Delta P \left[\frac{1}{4} \frac{\pi r^4}{\mu L} + \frac{k_a k_b A_a A_b}{\mu (k_b \Delta x A_b + k_a \Delta x A_a)} \right] \quad (3)$$

Which again becomes:

$$Q = \Delta P \left(\frac{1}{{4 \mu L}/{\pi r^4}} + \frac{1}{{\mu (k_a \Delta x A + k_b \Delta x A)}/{k_a k_b A^2}} \right) = \frac{\Delta P}{{4 \mu L (k_a + k_b)}/{((k_a + k_b) \pi r^4 + 4 k_a k_b A)}} \quad (4)$$

Equation (4) shows that the flow resistance of the matrix is inversely proportional to the product of both permeabilities and is dominated by the smallest permeability of the system

2.2. Experimental procedures

A recently built in-house HP-HT micromodel rig for use up to P=500 bar, T=150°C has been utilized, which makes use of a high pressure cell containing the micromodel. The flow cell is immersed in a mineral oil bath which is heated at the required temperature. Two experimental procedures have been utilized during the experimental work (table 3): the second one, used for the last 3 experiments, is an improved version and is the one which is described here. The authors consider that the modification in the protocol (made to enhance the robustness of the manipulation) has not changed the qualitative nature of the results and corresponding observations.

Without entering the details of single experiment P,T variations, the experimental procedure "EP2" (table 3) for a P=30 bar, T=60°C experiment, can be generalized as, referring to the scheme in figure 5:

1. Micromodel vertically placed
2. Pull the vacuum in all the circuit including the micromodel.
3. Open the valve V1 while V2, V3, V4 are closed and inject oil in the circuit from the bottom with the oil pump at P=2 bar, until the oil level reaches the top end.
4. Use the 'air' reservoir at P=30 bar to pressurize all circuit.
5. Open all valves to have P=30 bar everywhere.
6. Close V1 and V2 and maintain V3 open. Inject propane from «propane pump» to saturate dead volumes on top.
7. Finally inject propane at 100 µl/h until it enters the micromodel, opening V2 and closing V3.

An optical camera (Phase One) with a detector 10328x7760 pixels was used to capture images at a resolution of approximately 9 µm/pixel. This allows

Table 3. Experiment description list: EP is experimental procedure; SS is solvent state: gas, liquid, supercritical SC; the miscibility state (MS) for all the experiments is shown by comparison to the minimum miscibility pressure (MMP).

Exp N.	Chip N.	EP	SS	P bar	T °C	Q µl/h	S_{or} %	S_{wi} %	MMP bar	MS
1	1	1	Gas	8,5	60	100	~ 20	0	21.51	Immiscible
2	1	1	Liq	30	60	1000 - 100	~ 0	0		First Contact M.
3	1	1	Liq	100	60	100	~ 0	0		
4	1	1	Liq	30	60	100	~ 0	0		
5	1	1	SC	50	110	100	~ 10	0	50.74	Near Miscible
6	2	2	Liq	30	60	100	~ 0	~ 20	21.51	First Contact M.
7	2	2	Liq	30	60	100	~ 0	0		
8	3	2	Liq	30	60	100	> 80	0		

observing details at the pore scale whilst also imaging the full extension of the pore pattern (25cm^2). The image capture frequency was kept at a rate of 4 images/minute, which was the maximum possible capture rate for this large image size. From experiment 6 onwards, inlet/outlet channels were also almost completely captured in the images. A second camera (IMPERX) is used to capture a video of the experiment, mainly for QC purposes, at higher time resolution but lower spatial resolution.

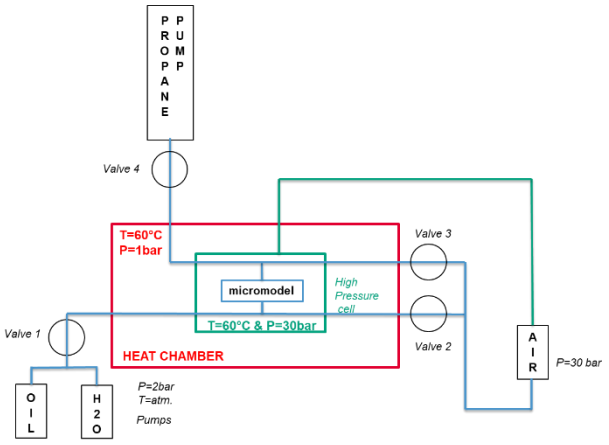

Fig. 5. Schematization of the experimental set-up for HP-HT micromodel experiments. Case of P=30 bar, T=60°C experiment.

2.2.1 Fluids

The fluids employed in the experiments were:

- Viscous oil (viscosity 135cp @ T=60° ; density 909kg/m^3; asphaltene content 4.4% weight)
- Solvent: Pure propane (P_{crit} : 42bars ; T_{crit}=97°C)
- Brine (45g/L Nacl, 5g/L CaCl)
- Air (Nitrogen)

Depending on the P, T conditions the solvent was injected as gas, liquid or supercritical state.

3 Organisation of experiments

Table 3 reports the characteristics of the 8 experiments. Residual oil saturation (Sor) is estimated qualitatively by visual inspection. Note that the rate in experiment 2 was of 1000 µl/h until solvent breakthrough, then dropped to 100 µl/h. Experiment 7 is the repetition of experiment 6 in exactly the same conditions, apart from presence of connate water, S_{wi}. Experiment 7 also repeats experiments 2 and 4 in terms of identical P,T conditions.

4 Interpretation of the experiments

4.1. Pore-level visual observations

The following general observations on the displacement can be made:

- No oil is trapped in the miscible tests, all is produced.
- Experiment 1 (immiscible, solvent in gas state) and experiment 5 (supercritical near miscible) both show trapped oil ganglia, but of different sizes (figure 6).
- At miscible conditions, precipitation of asphaltenes is normally observed (dark black phase in figure 7).
- Solvent breakthrough always takes place via a fracture, except for experiment 7, where instead a finger through the matrix travels faster than the one in the fracture (figures 8, 9).
- Experiment 8 has solvent flow only in fractures: the matrix is largely unaffected, with exception of the areas near the fracture (figure 10).

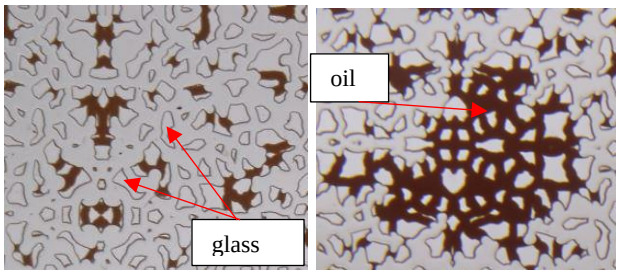

Fig. 6. Trapped oil configurations in experiment 5, left, (supercritical, near miscible) and experiment 1, right, (gas state, immiscible): in the latter larger blobs are present. See also figure 11 and 14.

4.2. Pressure and temperature

The definition of the miscible condition is the first aspect to define. Thus, for a given solvent, the temperature of the system defines the minimum miscibility pressure (MMP) that must be attained to have either multi-contact or first contact miscibility. These values were calculated with an in-house PVT software and the resulting miscible conditions are detailed in table 3.

In this section, experiments 1, 3, 4 and 5 (highlighted in orange in table 3) are specifically studied to observe how pressure and temperature conditions impact on the fluids behaviour (figures 11, 12, 13, 14). We observe that:

- The behaviour of the experiments changes drastically once the minimum miscibility pressure is achieved (first contact miscibility in these cases).
- The pressure in experiment 1 is below the MMP, by consequence oil gets trapped due to capillary forces. Solvent goes preferentially through the left fracture where the solvent breakthrough takes place rapidly. Oil keeps being produced until percolation takes place in all 3 fractures: only when all three fractures are conducting, the oil production stops. The residual oil is about 20%, located mostly at the bottom.
- The pressures of experiments 3 and 4 are above the MMP. Therefore, they are in first contact miscible regime and no capillary forces exist. All the oil is produced in these cases and fluids' behaviour is almost the same in both experiments.
- Experiment 5 retains approximately 10% of the oil. This is due to the presence of capillary forces that trap the oil. However, oil is produced quicker (less PVs of solvent injected) than for the first contact miscible experiments. The reduction of oil viscosity due to a higher temperature (110°C instead of 60°C) explains this observation. It might be considered too that, according to [13], capillary forces may be a source of mixing that enhance the oil recovery of dead-end pores while in near-miscible or multi-contact miscible conditions. The same effect is observed by [1] in their work with CO2 injection. Although controversial, this mechanism has been observed in several works [8, 9] and could be another reason to explain the observed behaviour.

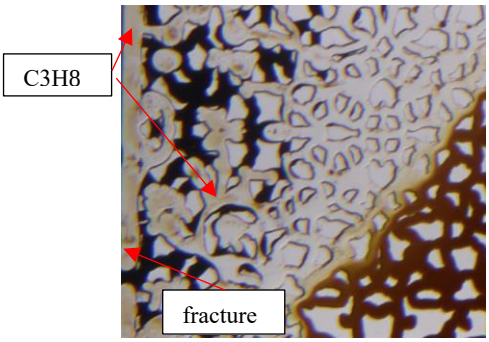

Fig. 7. "Black" asphaltene deposits at a late stage of experiment 2. The fracture is visible on the left hand side. The front of miscibility in the matrix is also seen (change in oil colour).

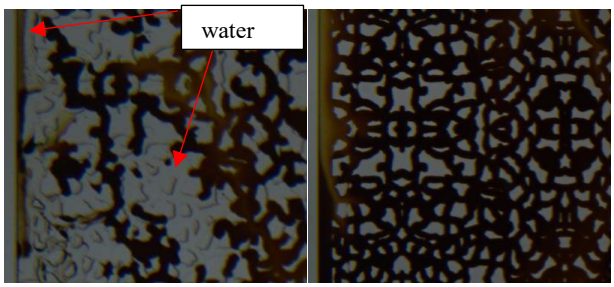

Fig. 8. Early stage of the experiments 6 and 7. Left: snapshot right after solvent breakthrough in fracture for experiment 6 (with Swi). Right: snapshot of solvent finger in fracture for experiment 7 (no S_{wi}), just seconds before the breakthrough, which will happen at another location.

Fig. 9. Moment of breakthrough for the solvent finger in experiment 7 which has travelled through the matrix (see also figure 17).

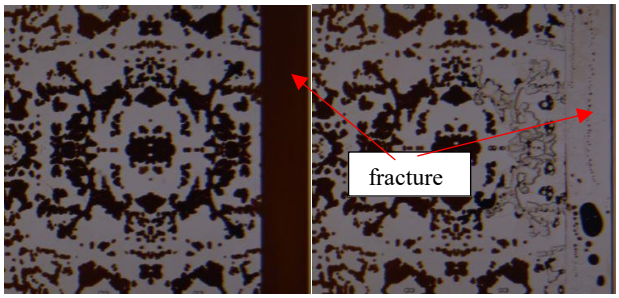

Fig. 10. Detail of the fracture region for experiment 8. The fracture is visible on the right. Left: snapshots at the start of the experiment. Right: at the end of the experiment after 1 day (right). The state remained nearly identical even after 13 more days of continuous solvent flooding.

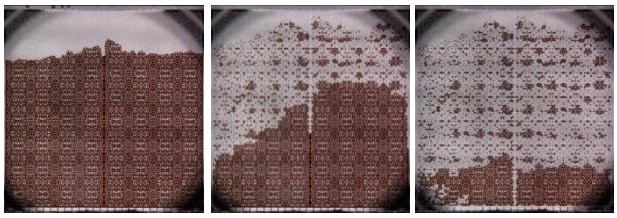

Fig. 11. Experiment 1 at different stages: from left to right, start of the test, after 4.38h and after 166.27h respectively, which in this case represents the very end of the experiment. Note that the right hand side image also represents the situation at the very end of the experiment: the matrix in the bottom part of the micromodel could not be swept. (Note: an instantaneous pressure fluctuation at the very start of the experiment made the oil level slightly raise which explains the different height of oil between the snapshot at the start and that after 4.38h).

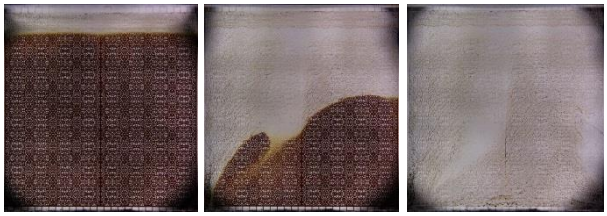

Fig. 12. Experiment 3 at different stages: from left to right, start of the test, after 1.2h, and after 3.32h respectively, at experiment completed. A finger developed at some point.

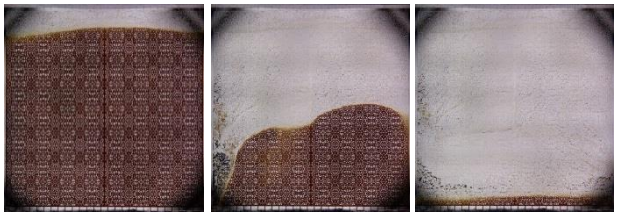

Fig. 13. Experiment 4 at different stages: from left to right, start of the test, after 0.43h and after 1.73h respectively, at experiment nearly completed.

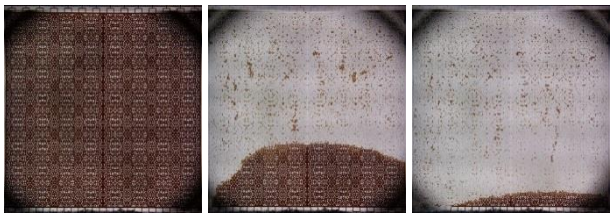

Fig. 14. Experiment 5 at different stages: from left to right, start of the test, after 0.28h and after 0.73h respectively, at experiment nearly completed.

4.3. Injection rate and amount of inlets/outlets

Experiments 2 (figure 16), 4 (figure 13) and 7 (figure 18) were performed at 30 bar and 60°C in the "sandstone-like" micromodel but with different injection rates (experiment 2 vs experiment 4) and with different inlets/outlets characteristics (experiment 7 vs experiment 4). The differences are detailed in table 4.

Table 4. Experimental details defining the peculiarities of experiments 2, 4 and 7.

Parameter	Exp. 2	Exp. 4	Exp. 7
Injection rate (µl/h)	1000 and 100 after solvent breakthrough	100	
Amount of inlets/outlets	28 narrower inlets/outlets		20 wider inlets/outlets

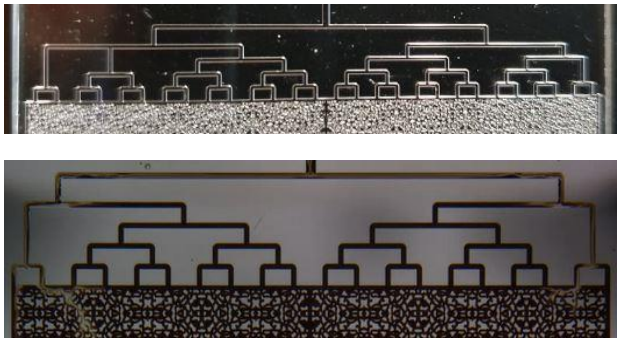

Fig. 15. Detail of inlet/outlet channels. Top image: 28 inlet/outlet channel configuration: this does not favour solvent entry through the sides. Bottom image: 20 inlet/outlet channel configuration: this tends to favour solvent entry via the sides (as can be seen, by the colour change).

The observations are:

- Experiment 2: Increasing injection rate (compared to experiment 4), whilst the viscosity ratio between oil and solvent is higher than 1000, has the sole effect of speeding up solvent breakthrough favouring the channelization. This is also observed by [4]. Nonetheless, the injection rate is decreased after the solvent breakthrough and the final performance becomes similar to that observed in experiment 4.
- The 28 inlet/outlet channel configuration does not favour solvent entry through the sides (as the 20 channel configuration does): nevertheless, solvent still travels via the edge of the micromodel (in the fractures).
- Experiment 7: Solvent fingers are clearly observed in the matrix and are parallel and close to the side fractures. Their growth is later damped by transverse dispersion but these early invaded zones control the solvent path through the matrix and contribute to the solvent breakthrough. This radically different behaviour of percolation in the matrix and not in fractures could be explained considering that experiment 7 has less but wider inlet channels. Thus, for the same total injection rate, each inlet has a higher "individual injection rate", which may trigger sustained finger growth in the matrix (see also section 4.6).

Fig. 16. Experiment 2 at different stages: start of the test, after 0.93h and after 2.1h, end of the experiment, from left to right.

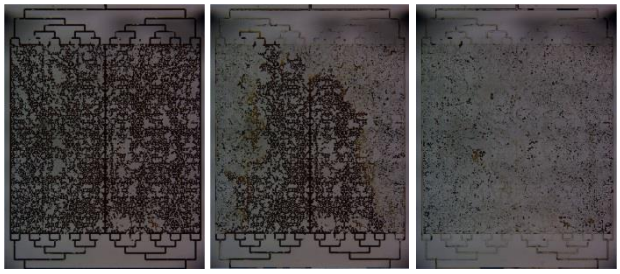

Fig. 17. Experiment 6 with Swi (Chip 2) at different stages: start of the test, after 5.6h and after 15.15h, from left to right.

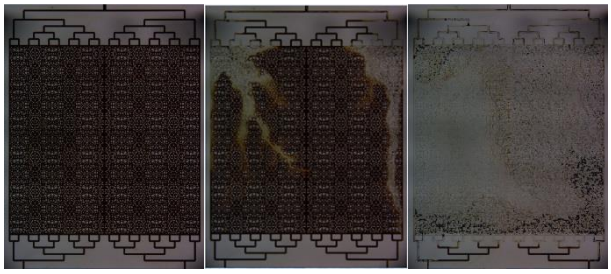

Fig. 18. Experiment 7 with no water (Chip 2) at different stages: start of the test, after 0.1h and after 2.0h, from left to right.

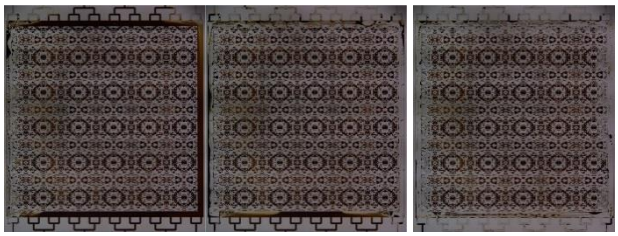

Fig. 19. Experiment 8 in Chip 3 ("Bi-modal carbonate-like") at different stages: start of the test, after 0.37h and after 16.32h, from left to right.

4.4. Immobile water presence

The effect of immobile water on miscible behaviour is studied comparing experiments 6 (figure 17, with connate water) and 7 (figure 18, without connate water), both performed on the same Chip 2. Both were performed at the same pressure and temperature, 30 bar and 60°C, which implies first contact miscible conditions. The main observations and conclusions are:

- The dynamics of oil recovery is slower. As the medium is water-wet, immobile water acts as a mass transfer barrier that retards the contact between oil and solvent and interrupts the mixing mechanisms. This is observed by several authors [2, 10, 14]. If the medium were oil-wet, then oil would wet the pore walls and form a film. This would allow the oil-solvent mass transfer through it. Consequently, water presence would not have a great impact on the mixing mechanisms as it does, on the contrary, on the water-wet media used here.
- On the other hand, early solvent channelization and breakthrough through the two lateral fractures is observed if S_{wi} is present (compared to experiment 7, without water). Considering equation (2), it is observed that decreasing the effective matrix cross sectional area of flow ('A'), which is now partially occupied with water, increases the matrix resistance for the solvent to flow. This favours the passage of solvent through the less resistance paths, which in this case are the two lateral fractures.

4.5. Comparison with double porosity, larger fracture case

Experiment 8 (figure 19) was performed in a bi-modal "carbonate-like" micromodel (Chip 3). It has two types of porosities, which we can define as macro- and micro-porosity. The latter connects the macro-pores with each other and to the rest of the medium. The observations are compared with those from experiment 7 ("sandstone-like", single-type matrix porosity, figure 18), which was performed at the same pressure and temperature conditions (30 bar and 60°C, implying first contact miscibility). The same experimental procedure (EP2) is used.

The main observations for experiment 8 are:

- Estimated residual oil is approximately 80%, even after 13 days of continuous solvent injection, and is very high compared to that of Experiment 7 which instead sweeps all the oil in 2.0 hours. Oil is only recovered at the lateral borders near the two lateral fractures, where solvent breakthrough was instantaneous: solvent goes through the fractures and barely invades the matrix.
- Almost no oil is produced after 30 minutes from the start of the experiment.
- Some mass transfer takes place between the fractures and the regions next to it.

This behaviour can be explained comparing equations (2) and (4) and considering the connectivity of the medium (production allocation in the matrix and the fractures) as well as the mixing mechanisms (matrix-fracture and matrix-matrix interactions), which are very different than those of Chips 1 and 2. The resistance to flow due to the fractures and matrix can be seen as:

$$\delta = \frac{R_{fractures}}{R_{matrix}} = \frac{{}^{8\,\mu\,L}/_{\pi r^4}}{{}^{\mu\,\Delta x}/_{k\,A}} = 8\,\frac{k\,A}{\pi r^4} \qquad (5)$$

Therefore experiment 7 ("sandstone-like") has a greater value of δ than experiment 8 ("carbonate-like"), consequence of a smaller fracture characteristic size and a bigger matrix permeability: experiment 8 has a

resistance ratio δ such that only production through the fractures prevails.
In terms of mixing mechanisms, considering equation (6),

$$\frac{D_{eff}}{D} = \frac{\emptyset}{\tau} \quad (6)$$

the effective diffusion coefficient for experiment 8 is smaller than for experiment 7 and the mass transfer by diffusion between the fractures and the matrix is slower as observed in the experiment.

Considering microscopic dispersion, since both transverse and longitudinal dispersion depend on the interstitial velocity (Perkins and Johnston [15]), which is practically zero inside the matrix for experiment 8, then dispersion mechanisms must be absent inside the matrix. However, the zones of the matrix next to the fractures have a higher interstitial velocity and then, the diffusion coefficient plays a role. According to the discussion in [15], the mixing mechanisms that take place in the zones next to the fractures are diffusion dominated and very slow.

On top of the observations above it is worthy reporting that solvent is again percolating preferentially through the left hand side fracture: this general behaviour of our experiments might be due to a slight tilting of the vertically positioned micromodel.

4.6. Viscous fingering analysis

Viscous fingering refers to the onset and evolution of morphological instabilities that occur at the interface of two fluids while they displace each other in a porous medium. Their formation and growth depends on the balance of viscous and gravity forces, the dispersion mechanisms and the heterogeneities of the medium. These three parameters are analysed in order to understand the results of these experiments. Gravity forces may improve the sweepout and oil recovery by preventing an early breakthrough of the lighter solvent and the formation of bypassed areas. This is achieved when the solvent is injected from the top and the production rate (equal to the injection rate in these cases) is low enough for gravity to keep solvent and oil segregated, avoiding the formation of the solvent fingers. In order to define the stability of the displacement, the injection rate of all the experiments was compared to the critical velocity defined by Dumoré [16] in:

$$u_c = \frac{(\rho_o - \rho_s)}{(\mu_o - \mu_s)} k * g = Critical\ velocity \quad (7)$$

The expression above was developed assuming that injection is from the top, the solvent/oil interface is horizontal with a negligible transition zone. According to this criterion, the injection rate (100ul/hr, resulting in 5,96 ft/day) is too rapid, that is, higher than the critical velocity, which is less than 1 ft/day for any of our experiments: it means all the experiments should show solvent fingers as buoyancy is not strong enough to prevent their initiation and growth by viscous/advection forces. On the other hand, instabilities in the matrix were only observed in two experiments (for example, experiments 7, figure 18). This behaviour can be explained due to the contributions of the transverse dispersion (which smooths out the fingers as they grow) and to the stabilizing role of the fractures, in relation to the flow inside the matrix. The presence of fractures simply reduces the effective flow rate inside the matrix, as fractures and matrix compete in the production of oil (parallel system). In other words the actual velocity in the matrix is slower than the injection rate, and therefore the system tends to stabilize, i.e. we don't observe fingers in the matrix.

5 Simulation exercise on "sandstone-like" pattern

We finally report a simulation exercise whose objective is to verify that the set of equations embedded in the simulator is able to reproduce the obtained experimental results, with the available information, and even at these small scales. This is a two edge situation in which both equation system and data must prove to be adequate, since a unique set of inputs must be able to reproduce the different observations as P,T change. The benefit of adding this study is to give confidence in future sensitivity analysis that can be run to forecast possible outcomes and propose future experimental set-ups, even at core scale.

The simulator STARS CMG was used. For the construction of the grid, the values of matrix permeability for the Chip 1 and 2 were obtained numerically by means of the Stokes solver OPENFOAM applied to a segmented portion of the chip, as seen in figure 20 [17]. The permeability was estimated to be around 42D, which should be considered a qualitative estimate also in light of the large uncertainty on the segmentation of the experimental image. Porosity used in the grid for the matrix is 66%. The diffusion coefficient was estimated from published data for similar solvent types as D= 2.7*10-7 m^2/day.

Simulations were not carried out for Chip 3 (experiment 8) as it was not possible to obtain the permeabilities of the matrix, "macro-" and "micro-porosities".

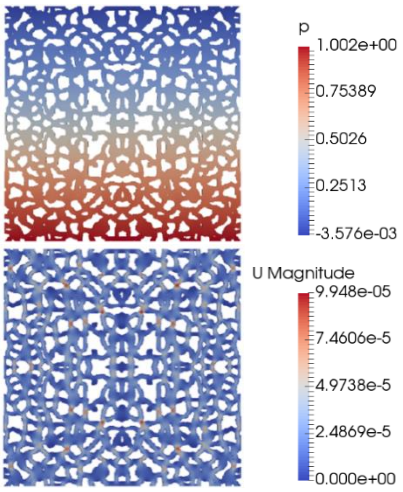

Fig. 20. CFD simulation on a sample from the Chip 1 (2): pressure field on top; velocity field at the bottom. Legend in SI units (for an arbitrary pressure drop of 1 Pa across the model).

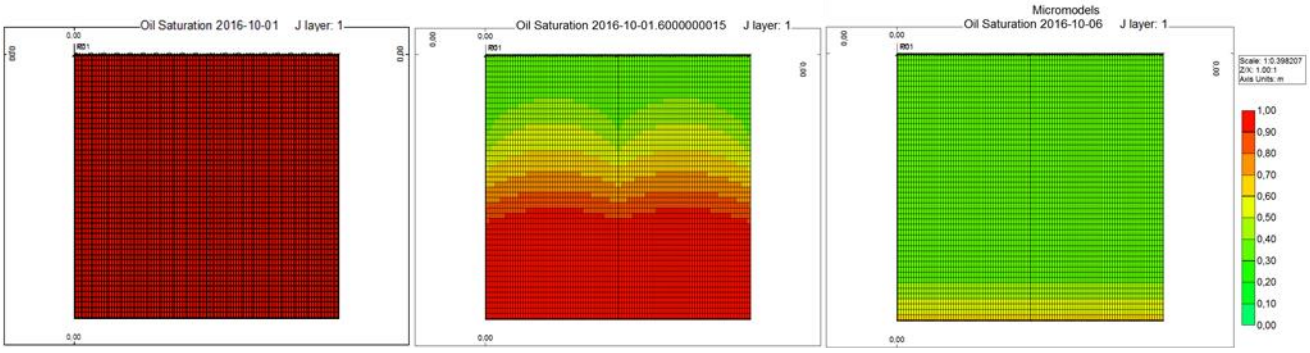

Fig. 21. Experiment 1 (P=8.5 bar; T=60°C) flow simulation. Oil saturation at different stages (after 0 days, 0.6 days, and 5 days).

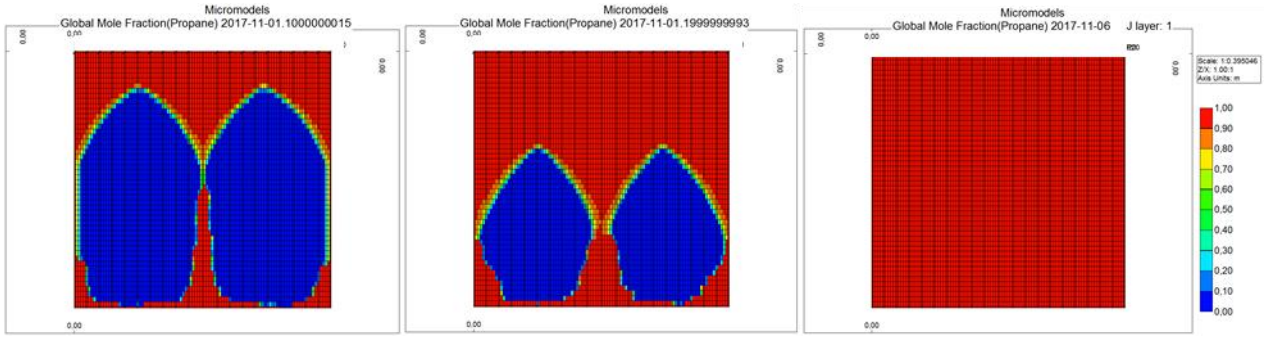

Fig. 22. Experiment 3 (P=100 bar; T=60°C) flow simulation. Global mole fraction of propane at different stages (after 0.1 days, 0.19 days, and 5 days).

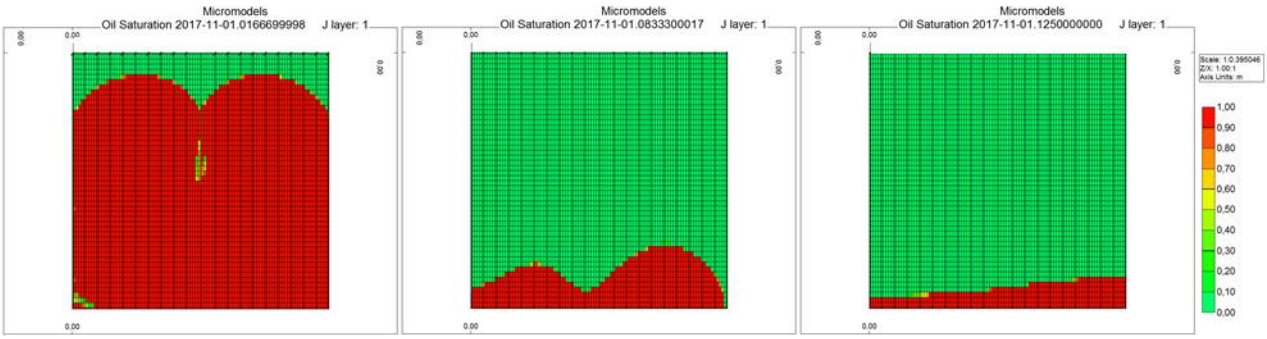

Fig. 23. Experiment 5 (P=50 bar; T=110°C) flow simulation. Oil saturation at different stages (after 0.01 days, 0.08 days and 0.12 days).

5.1. Experiment 1 (P=8.5 bar; T=60°C)

It was decided to simulate experiment 1 with one "producer" and one "injector well" (using common reservoir engineering terminology that will also be used in the next two paragraphs), to mimic the chip's inlet/outlet ports. Capillary pressure and relative permeabilities were taken into account because it is an immiscible displacement case. This simulation could not reproduce the complex dynamics of experiment 1 (figure 21): as mentioned above, there is some residual oil left (in the form of a bottom layer) at the end of the experiment. In the simulation, the solvent does not percolate through the fractures in the same (complex) way as instead it does in the experiment. In the experiment the left fracture is first percolated, followed by the right fracture and finally the central one: only when the total conductivity of the fractures is large enough, the matrix is cut out. In the simulation, the solvent front gets only deformed by the fractures.

5.2. Experiment 3 (P=100 bar; T=60°C)

The numerical set-up includes now 20 "producers" and 20 "injectors": this change allowed to better represent the visual "history of production" for this experiment. The relative permeabilities are considered as equal to the phase saturation [14] for first contact miscibility cases (experiments 3, 4, 6 and 7). Observations: all the oil is recovered as observed in the experiment. It was later also verified that relative permeabilities do not impact flow in the simulation: this is because the solvent, propane, is a liquid and the simulator solves the case as monophasic flow of liquid oil. This is also why figure 22 shows the global mole fraction of propane instead of the oil saturation. The same exercise was conducted to reproduce the experiment 4 (P=30 bar; T=60°C) leading to nearly

identical outcome as well as for Experiment 6, where connate water was not seen to change the picture (cases not reported here).

5.3. Experiment 5 (P=50 bar; T=110°C)

This is the experiment performed in supercritical conditions. The numerical set up is similar to the previous case as well as the relative permeabilities. Capillary pressure is not taken into account because CMG STARS has convergence problems (so it is then set to "zero" for any saturation). A residual oil saturation of 8% was obtained, similar to the experiment. The asymmetry seen in figure 23 is due to a negative skin attributed to the wells on the left side, in order to try to represent as close as possible the experimentally observed asymmetry.

Overall the simulation exercise conducted at these small scales has proven that it is possible to reproduce the main qualitative features of the experiments.

5 Conclusions

The topic of investigation of this paper has been the injection of a solvent (propane) in viscous oil using HP-HT glass micromodels.

The experiments show that for an isothermal process, for a given pore pattern and solvent, pressure modifies drastically the displacement behaviour, as an indication of how far the oil-solvent system is from miscibility. A miscible displacement is observed once the miscibility pressure is surpassed. Above that value, the behaviour of the system will not change any more as long as pressure stays in the range of multi-contact miscibility or first contact miscibility.

Water presence, for the water-wet media used in this work, acts as a barrier to solvent-oil contact and affects the apparent pore size distribution available for solvent flow paths and mass exchange. The effective matrix cross sectional area available to flow becomes now partially occupied with water, increasing the matrix resistance for the solvent to flow (whilst fractures have remained water-free during oil drainage) and the recovery becomes slower. However, the overall performance does not change as all oil is recovered despite the water presence.

An important effect of fracture characteristic size was seen. The ratio between fracture and matrix permeability is considered to have highly affected the displacement efficiency: once a certain threshold is surpassed, the recovered oil drops drastically despite being a miscible displacement. This can also happen once solvent has broken through a high enough number of fractures, as seen in the immiscible case (experiment 1). These behaviours can be hard to predict a priori.

According to criteria defined in the literature, the experiments are classified as having unstable displacement. By consequence, solvent fingers are expected as buoyancy is not strong enough to prevent their initiation and growth by viscous/advection forces. But this happened to be the case only in a minority of experiments. This behaviour is explained as being a consequence of the contributions from transverse dispersion (which smooths out the fingers as they grow) and from the presence of fractures which in fact aid in stabilizing the character of the flow inside the matrix, since they "absorb" most of the instability. Changes in inlet boundary conditions from one chip to another also play a role.

Finally a numerical simulation exercise with CMG STARS simulator was conducted which allowed to qualitatively reproduce the main behaviours observed in the experiments, with a unique set of petrophysical and PVT inputs. There is a hint though that complex fracture matrix completion might not be easily predictable by simulation, as it was the case for experiment 1. Nevertheless, this exercise being satisfactory, it provides confidence for future numerical applications.

The authors would like to acknowledge TOTAL for permission to publish this paper and Drs Clément Varloteaux and Igor Bogdanov (CHLOE) for the technical discussions and help on simulation. Richard Rivenq (TOTAL) is also gratefully acknowledged for improving the quality of the manuscript with his comments.

Nomenclature

Q = total flow rate, m^3/s
ΔP = delta pressure, Pa
r = fracture one chracateristic size, m
L = fracture and pore pattern length, m
μ = oil viscosity, Pa.s
k = permeability of the matrix, m^2
A = matrix cross sectional area of flow, m^2
Δx = matrix length through which ΔP is measured, m
k_a = permeability of the macropores, m^2
k_b = permeability of the micropores, m^2
D_{eff} = effective diffusion coefficient, m^2/s
D = bulk diffusion coefficient, m^2/s
Ø = fractional porosity, dimensionless
τ = tortuosity, dimensionless
ρo, ρs = oil and solvent density, kg/m^3
μo, μs = oil and solvent viscosity, Pa.s
g =standard acceleration due to gravity = 9.81 (m^2/s)

References

1. I. Chatzis, Pore scale phenomena of heavy oil recovery using vapor extraction, SCA n° 2002-26, *Society of Core Analysts*, Monterey, CA, USA, (2002)
2. B.T. Campbell and F. M. Orr Jr, Flow Visualization for CO2/Crude-Oil Displacements, *Society of Petroleum Engineers*, https://doi.org/10.2118/11958-PA (1985)
3. M. Sohrabi, A. Emadi, M. Jamiolahmady, S. Ireland, C. Brown, Mechanisms of extra-heavy oil recovery by gravity stable CO2 injection, SCA n° 2008-20, *Society of Core Analysts*, Abu Dhabi, UAE (2008)
4. M. Saidian, M. Masihi, M. H. Ghazanfari, R. Kharrat, S. Mohammadi, An Experimental Study of the Matrix-fracture Interaction During Miscible Displacement in Fractured Porous Media: A

Micromodel Study, *Energy Sources, Part A: Recovery, Utilization, and Environmental Effects*, 36:3, 259-266, https://doi.org/10.1080/15567036.2010.536828 (2014)

5. F. Civan, *Porous media transport phenomena* (Wiley, 2011)
6. A. Marciales, T. Babadagli, Pore scale visual investigations on solvent retrieval during oil recovery at elevated temperatures: A micromodel study, *Chemical Engineering Research and Design,* Vol. 106, 59-73, https://doi.org/10.1016/j.cherd.2015.12.007 (2016)
7. Y. H. Shokrlu, T. Babadagli, Pore-Scale Investigation of Phase Distribution and Residual-Oil Development During Secondary and Tertiary Solvent Injection, *SPE Reservoir Evaluation & Engineering, 18, 01, https://doi.org/10.2118/173180-PA (2015)*
8. Z. Qi, A. Abedini, P. Lele, N. Mosavat, A. Guerrero, D. Sinton, Pore-scale analysis of condensing solvent bitumen extraction, *Fuel*, 193, 284-293, https://doi.org/10.1016/j.fuel.2016.12.070 (2017)
9. J. E. Burger, K. K. Mohanty, Mass transfer from bypassed zones during gas injection, *SPE Reservoir Engineering,* 12, 02, https://doi.org/10.2118/30768-PA (1997)
10. P. Wylie, K. K. Mohanty, Effect of Wettability on Oil Recovery by Near-miscible Gas Injection. *Society of Petroleum Engineers,* doi:10.2118/39620-MS, https://doi.org/10.2118/39620-MS (1998)
11. K. M. Hopstaken, The effect of miscibility conditions on Gas Oil Gravity Drainage; an experimental study in a simulated fractured medium using CO2 as a displacement agent, *Msc Thesis*, Faculty of Geosciences, Utrecht University, https://dspace.library.uu.nl/handle/1874/278654 (2013)
12. M. S. Ameen, Fracture and in-situ stress patterns and impact on performance in the Khuff structural prospects, eastern offshore Saudi Arabia, *Marine and Petroleum Geology,* Vol. 50, Pages 166-184 (2014)
13. G. V. Chilingarian, S. J. Mazzullo, H. H. Rieke, Carbonate reservoir characterization: a geologic-engineering analysys, part I, *Developments in petroleum science* 44 (Elsevier, 1992)
14. F. I. Stalkup Jr, Miscible displacement, *SPE Monograph and Richardson*, Society of Petroleum Engineers (1983)
15. T. K. Perkins, O. C. Johnston, A review of diffusion and dispersion in porous media, *SPE J.*, 3, 1, (1963)
16. J. M. Dumoré, Stability considerations in downward miscible displacement, *SPE Journal*, 356-317 (1964)
17. C. Varloteaux, I. Bondino, I. Bogdanov, Rock absolute permeability analysis using image-based direct pore-scale simulations. *InterPore 10th Annual Meeting and Jubilee*, May 14 – 17 2018, New Orleans, LA (2018)